Journal of Molecular Catalysis A: Chemical 329 (2010) 27–35

Contents lists available at ScienceDirect

Journal of Molecular Catalysis A: Chemical

journal homepage: www.elsevier.com/locate/molcata

EXAFS investigation of the morphology of immobilized $Rh(PPh_3)_3Cl$ on phosphinated MCM-41

Jen-Ray Chang[a], Hsiu-Mei Lin[b], Sheau-Wen Cheng[c], Chia-Kai Tseng[c], Der-Lii Tzou[c], Shin-Guang Shyu[c,d,*]

[a] Department of Chemical Engineering, National Chung Cheng University, Taiwan, ROC
[b] Institute of Bioscience and Biotechnology, National Taiwan Ocean University, Taiwan, ROC
[c] Institute of Chemistry, Academia Sinica, Taiwan, ROC
[d] Department of Chemistry, National Central University, Taiwan, ROC

ARTICLE INFO

Article history:
Received 12 April 2010
Received in revised form 9 June 2010
Accepted 10 June 2010
Available online 17 June 2010

Keywords:
Mesoporous materials
$Rh(PPh_3)_3Cl$
Hydrogenation
Solid state NMR
EXAFS

ABSTRACT

$Rh(PPh_3)_3Cl$ was immobilized on a $(OEt)_3Si(CH_2)_3PPh_2$ modified MCM-41 to form a stable hydrogenation catalyst. The morphology of the catalyst was characterized by X-ray absorption spectroscopy. The EXAFS results indicates that the immobilized Rh catalyst has an average Rh–O_s (O_s is a surface oxygen) and Rh–Si bond distances of 2.01 Å and 3.15 Å, respectively, suggesting that monomeric Rh complex bonds to the MCM-41 surface. However, the structure of the immobilized Rh complex is not retained after hydrogenation of cyclohexene at 75 °C under 150 psi of H_2. After the reaction, the presence of Rh–Rh contribution with average bond distance of 2.68 Å and coordination number of 1.3 and the missing contribution with bond distance of 3.85 Å suggest that the reaction induces the coalescence of Rh complex to form dimeric Rh species. However, formation of trace amount of Rh metal clusters cannot be ruled out because rather small characteristic peak for the missing Rh–Rh shell may be covered by noise.

1. Introduction

Immobilization of homogeneous catalysts to form recoverable catalysts by anchoring catalysts (usually metal complexes) on solid supports has been studied extensively in the past four decades [1–4]. Recently, using mesoporous materials as catalyst supports has been intensively investigated due to their large regular pore size and high surface area [5,6]. Large pore of the materials allows passage of large molecules such as organic reactants and metal complexes through the pores to reach to the surface of the channel [7–12]. The regular pore size can provide shape selectivity, which cannot be provided by silica gel.

We have communicated the immobilization of $Rh(PPh_3)_3Cl$ on phosphinated MCM-41 for catalytic olefin hydrogenation [13]. This catalyst has a higher TOF (turnover frequency) than that of $Rh(PPh_3)_3Cl$ under similar reaction condition. It is rather robust; leaching of Rh is limited and its catalytic activity remains intact after 20 recovery cycles with total TON (turnover number) greater than one million. Recently, several research groups have reported similar phenomena for other immobilized Rh catalyst systems with low leaching rates and high activities [14–18]. However, reasons for the low leaching rates, high activities, and high stability maintenance of these hybrid catalysts are still not reported.

In general, the immobilized catalyst is expected to reserve the structure of its parent complex, and its catalytic activity is also expected to be preserved. In this study, the robust property of the hybrid catalysts may be caused by the formation of complex-support bonding [19], while the increase of catalytic activity suggests a restructuring of the Rh complexes. Since EXAFS (extended X-ray absorption fine structure) provides the structural information characterizing surface-bounds complex, it offers the opportunities to understand how structure influences the leaching rate and catalytic properties. Herein, we report the EXAFS analysis of this hybrid catalyst to reveal the morphology of the immobilized Rh species before and after reaction.

2. Experimental

2.1. General procedures

All reactions and other manipulations were performed by use of standard Schlenk techniques under an atmosphere of nitrogen. MCM-41 was prepared by literature procedures [20,21]. Commercially available chemicals were purchased and used without further purification. Diphenylphosphine and n-butyllithium (1.6 M,

* Corresponding author at: Institute of Chemistry, Academia Sinica, 128 Academia Road, Sec. 2, Taipei 115, Taiwan, ROC. Tel.: +886 2 27898592; fax: +886 2 27831237.
E-mail address: sgshyu@chem.sinica.edu.tw (S.-G. Shyu).

1381-1169/$ – see front matter © 2010 Elsevier B.V. All rights reserved.
doi:10.1016/j.molcata.2010.06.013

hexane) were purchased from Aldrich. Rhodium triphenylphosphine chloride was from Strem. 3-Bromopropyltrichlorosilane was from Fluka. All solvents (except ethanol) were dried with Na and benzophenon under N_2 and distilled immediately prior to use. For powder X-ray diffraction, ICP-AES and BET surface area measurements, samples were dried at 60 °C in air before analysis. ^{1}H and ^{31}P NMR spectra were obtained on a Bruker Ac-300 spectrometer. ^{31}P NMR shifts are referenced to 85% H_3PO_4. Solid state ^{31}P NMR spectra were obtained on a Bruker (Avance 300) spectrometer. Microanalyses were obtained on a PerkinElmer 2400 CHN analyzer. BET surface area measurements were recorded on an ASAP 2010. Powder X-ray diffractions were recorded on a Siemens D5000 or a Philips X'Pert Pro X-ray diffractometer. Energy-dispersive spectra (EDS) were recorded on a scanning electron microscope (JSM-5400) equipped for energy-dispersive X-ray spectrometer (eXL, Link Systems). Wavelength-dispersive spectra (WDS) were recorded on a JEOL EPMA (Electron Micro-Probe Analyzer) JXA-8900R in the Institute of Earth Sciences, Academia Sinica. Gas products were analyzed by using a Hewlett Packard 6890 gas chromatograph. ICP-AES spectra were recorded on a Varian 720-ES spectrometer. Digestion of the hybrid catalyst was first carried out in a mixture of H_2O_2/HNO_3 solution with a MARS-5 CEM microwave digester at 180 °C under the power of 560 W then with HF (40%) solution to dissolve the remaining undigested SiO_2 materials.

2.2. $(OEt)_3Si(CH_2)_3Br$

A solution of 20.0 ml of absolute ethanol and 22.5 ml (16.3 g, 16.1 mmole) of triethylamine in 100.0 ml of benzene was cooled in an ice bath. A solution of 4.0 ml (6.4 g, 25.3 mmole) of $Br(CH_2)_3SiCl_3$ in 25 ml of benzene was added dropwise into the above solution in an interval of 25 min. The mixture was allowed to stir for 1 h and was then filtered. Solvent was removed from the filtrate. Further vacuum distillation at 50 °C under 4 mtorr obtained 5.8 g of $(OEt)_3Si(CH_2)_3Br$. Yield: 81.6%. Anal. calcd for $C_9H_{21}BrO_3Si$: C, 37.90; H, 7.42; Found: C, 37.48; H, 7.59. MS(FAB): M^++H m/z 285.0522. ^{1}H NMR($CDCl_3$): δ 3.79 (q, J_{HH} = 7.2 Hz, 6H, $SiOCH_2-$), 3.38 (t, J_{HH} = 6.9 Hz, 2H, $BrCH_2-$), 1.86 (m, 2H, $BrCH_2CH_2-$), 1.20 (t, J_{HH} = 6.9 Hz, 9H, $SiOCH_2CH_3$), 0.61 (m, 2H, $-CH_2Si(OEt)_3$).

2.3. $(OEt)_3Si(CH_2)_3PPh_2$

At room temperature, 8.7 ml of n-BuLi (1.6 M/Hexanes, 13.9 mmole) was added to a solution of 1.5 ml (1.6 g, 8.6 mmole) of diphenylphosphine in 18.0 ml of THF. After stirring for 3 h, 2.0 ml (2.6 g, 9.1 mmole) of $(OEt)_3Si(CH_2)_3Br$ was added into the above solution. The mixture was allowed to stir for additional 96 h. Solvent was then removed by vacuum, and a milky viscous liquid was obtained. Unreacted diphenylphosphine was removed from this viscous liquid by vacuum distillation at 100 °C under 1 mtorr. The residue was extracted with hexane. After filtration, a white solid and a yellowish filtrate were obtained. Hexane was then removed from the filtrate by vacuum, and 1.3 g of a yellow liquid of $(OEt)_3Si(CH_2)_3PPh_2$ was obtained. Yield, 35.6%. Anal. calcd for $C_{21}H_{31}O_3PSi$: C, 64.59; H, 8.00; Found: C, 64.64; H, 7.70. MS(FAB): M^++H m/z 391.1858. ^{31}P NMR(THF): δ −18. ^{1}H NMR($CDCl_3$): δ 7.42–7.24 (m, 10H, PPh), 3.78 (m, 6H, $SiOCH_2-$), 2.03 (m, 2H, PCH_2CH_2-), 1.50 (br, 4H, $PCH_2CH_2CH_2-$), 1.18 (t, J_{HH} = 7.0 Hz, 9H, $-SiOCH_2CH_3$), 0.60 (m, 2H, $-CH_2Si(OEt)_3$).

2.4. Preparation of MCM-41-P

MCM-41 was reacted with water at refluxing temperature for 4 hrs or at room temperature for 10 hrs. Water is removed by filtration, and the mesoporous powder was dried in an oven at 60 °C overnight to remove the surface H_2O. A surface silanol saturated MCM-41 (denoted as MCM-41-H_2O) was obtained as a white powder. MCM-41-H_2O (1.0 g) was placed into a round bottle Schlenk flask, and the system was flashed with nitrogen by evacuation and refilling process three times. Freshly distilled benzene (30.0 ml) and 1.0 ml (1.0 g, 2.4 mmole) of $(OEt)_3Si(CH_2)_3PPh_2$ were added into the flask and was heated to reflux for 4 h. The azeotrope ethanol/benzene (10.0 ml) was removed by distillation during the reaction. The mixture was cooled to room temperature, and additional 10.0 ml of benzene was added. The mixture was then heated to reflux for another 4 hrs, and another 10 ml of azeotrope was removed. The above procedure was repeated for four times. Totally 50.0 ml of azeotrope was removed. The mixture was then filtered, washed with $CHCl_3$, and dried in air at room temperature. The resultant white powder (denoted as MCM-41-P) was characterized by powder X-ray diffraction, EDS, and solid state ^{31}P NMR.

2.5. Preparation of MCM-41-Rh

A solution of $Rh(PPh_3)_3Cl$ (128.8 mg) in 10 ml of toluene was added to 0.5 g of MCM-41-P under nitrogen at room temperature. The mixture was stirred for one week and was then filtered. The resultant yellow powder was first washed with toluene then $CHCl_3$ until the filtrate was colorless. The yellow hybrid catalyst (0.5 g), denoted as MCM-41-Rh, was dried at room temperature in air and was characterized by powder X-ray diffraction, EDS, ICP-AES and solid state ^{31}P NMR.

2.6. Hydrogenation reaction

All the hydrogenation reactions were carried out in a 600 ml stainless steel Parr reactor equipped with a mechanical stirrer and a pressure transducer. In a typical hydrogenation experiment, catalyst, olefin (fleshly distilled), and solvent (toluene) were charged in the reactor under the flushing of nitrogen. The reactor was flushed with hydrogen after the reactor was closed. The autoclave was then charged with hydrogen (150 psi) and was heated up to 75 °C for 2 h. The reactor was then quickly cooled to room temperature by placing the reactor into an ice bath. The resultant mixture was filtered by filter paper to separate the heterogeneous catalyst from the solution. The filtrate was allowed to run through a small column of silica gel to remove any possible leached Rh species. The yield of the reaction was determined by analyzing the above filtrate by GC using a Hewlett Packard 6890 gas chromatograph equipped with a 30 m × 0.25 mm i.d. HP-5MS column.

2.7. Solid state NMR experiments

Solid state ^{31}P NMR spectra were acquired using a Bruker (Rheinstetten, Germany) Avance 300 MHz NMR spectrometer, operating at a proton/phosphate frequency of 300.13/121.49 MHz at ambient temperature. All the ^{31}P spectra were acquired by one-pulse experiment with rf field strength of 78 kHz. MAS frequency was set to 10 kHz with a recycle delay of 5 s. ^{31}P chemical shifts were referenced to the isotropic chemical shift of H_3PO_4 at 0 ppm.

2.8. X-ray absorption spectroscopy (XAS)

All X-ray absorption spectra of the Rh K-edge were measured on the beam line BL12B2 at SPring-8 [22] in Japan with storage ring energy 8 GeV and a beam current between 75 mA and 100 mA. The EXAFS measurements were performed in transmission mode at the X-ray Wiggler beam line with a double-crystal Si (3 1 1) monochromator. The higher X-ray harmonics were minimized by detuning the double-crystal monochromator to 80% of the maximum. The ion chambers used for measuring the incident (I_0) and transmitted (I) synchrotron beam intensities were filled with pure argon gas.

Table 1
d(1 0 0) spacing, pore size, pore volume and surface area of MCM-41, MCM-41-P, MCM-41-Rh and MCM-41-RhH.

	d(1 0 0) spacing (Å)[a]	Pore size (Å)[b]	Pore volume (cm^3/g)	BET surface area (m^2/g)
MCM-41	38.8	27.0	0.94	1028
MCM-41-P	38.1	18.0	0.40	588
MCM-41-Rh	38.0	17.5	0.24	304
MCM-41-RhH	37.0	18.0	0.24	306

[a] Powder X-ray diffraction.
[b] N_2 absorption–desorption isotherm.

Data reduction and data analysis were performed with the XDAP code developed by Vaarkamp et al. [23]. Standard procedures were used to extract the EXAFS data from the measured absorption spectra. The pre-edge was approximated by a modified Victoreen curve [24,25], and the background was subtracted using cubic spline routines [24–27]. Normalization was performed by dividing the data by the height of the absorption edge at 50 eV above the edge [24,25].

The EXAFS analysis for MCM-41-Rh and MCM-41-RhH was based on phase shifts and backscattering amplitudes determined either experimentally from the materials of known structure or theoretically by the use of FEFF [28,29] Reference functions of Rh–Rh and Rh–Si were generated by FEFF8, while Rh–P and Rh–O were obtained from EXAFS spectra of $Rh(PPh_3)_3Cl$ and Rh_2O_3.

For the reference functions of Rh–O, the Rh–O contribution was isolated from higher coordination shell by Fourier filter in the *k* range of 2.67–15.69 $Å^{-1}$ and *R* range of 0–2.1 Å. For obtaining the reference functions of Rh–P, the isolation procedure was more complex. In the Fourier transform of EXAFS spectra for $Rh(PPh_3)_3Cl$ (Fig. 4), The first contribution is from three phosphorus atoms of PPh_3 ligand and the second from one chlorine atom of chloride ligand. Since these two contributions couple with each other, they could not be separated by Fourier filter. Rh–P and Rh–Cl contributions were first calculated using the phase and amplitude functions obtained from FEFF 8. With difference file technique, these two contributions were further refined by calculating an EXAFS function that agrees as closely as possible with the experimental results. The phase shift and amplitude function was then extracted from the calculated EXAFS function of Rh–P. By use of reference functions extracted from experimental EXAFS spectra, the effects of low frequency noise on the accuracy of the structure-parameter estimation can be minimized.

3. Results and discussion

3.1. Preparation and characterization of the hybrid catalyst support

MCM-41 was prepared by the hydrothermal reaction of SiO_2 and $CH_3(CH_2)_{15}N(CH_3)_3Br$ [20,21]. It has a mesoporous structure with 1028 m^2/g BET surface area, 27.0 Å uniform pore size and 38.8 Å *d*(1 0 0) spacing in its powder X-ray diffraction (Table 1).

Condensation reaction between Si–OH and Si–OR forms the Si–O–Si linkage. Phosphine ligand $(OEt)_3Si(CH_2)_3PPh_2$ could therefore be attached to the MCM-41 surface through the condensation reaction between the Si–OR of the phosphine ligand and the Si–OH on the MCM-41. Silanol Si–OH groups on the surface of MCM-41 act as anchoring sites for the attachment of the phosphine ligand $(OEt)_3Si(CH_2)_3PPh_2$. In order to maximize the number of silanol groups, MCM-41 was first treated with water [30]. The resultant MCM-41 (denoted as MCM-41-H_2O) further reacted with $(OEt)_3Si(CH_2)_3PPh_2$ to produce a phosphinated MCM-41 (denoted as MCM-41-P) as illustrated in Scheme 1 [31,32].

Condensation reaction between Si–OH and Si–OR to form the Si–O–Si linkage is reversible. In favor of the formation of Si–O–Si linkage, $(OEt)_3Si(CH_2)_3PPh_2$ reacted with MCM-41-H_2O in benzene at refluxing temperature. Ethanol was removed by the distillation of the ethanol/benzene azeotrope during the reaction to avoid the reverse reaction [30]. A phosphine contained MCM-41 (denoted as MCM-41-P) was obtained in a white powder form.

The MCM-41-P has preserved its mesoporous character as indicated by its powder X-ray diffraction showing a 38.1 Å *d*(1 0 0) spacing (Fig. 1). The BET surface area is greatly reduced by half (588 m^2/g) with a 18.0 Å uniform pore size. The energy-dispersive

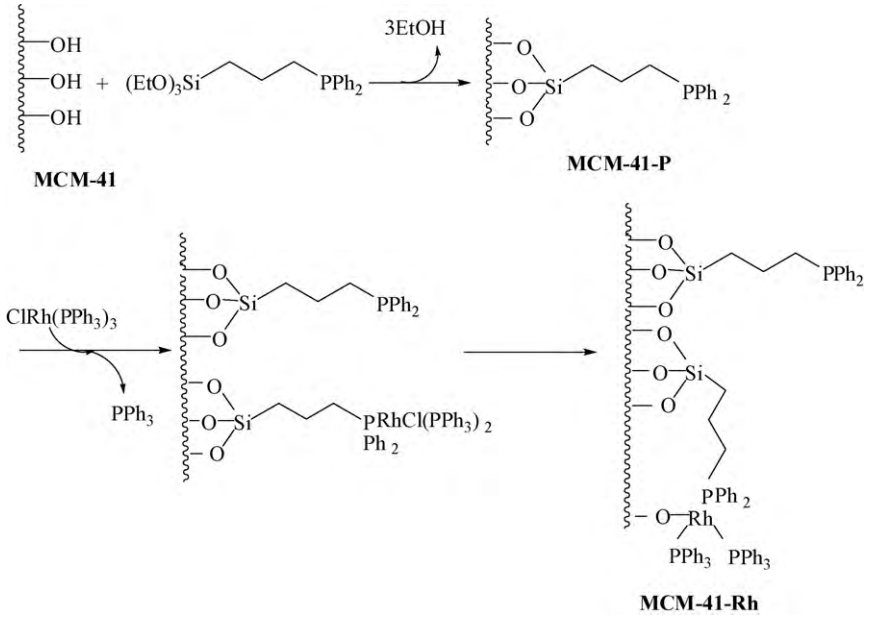

Scheme 1. Immobilization of $Rh(PPh_3)_3Cl$ on MCM-41.

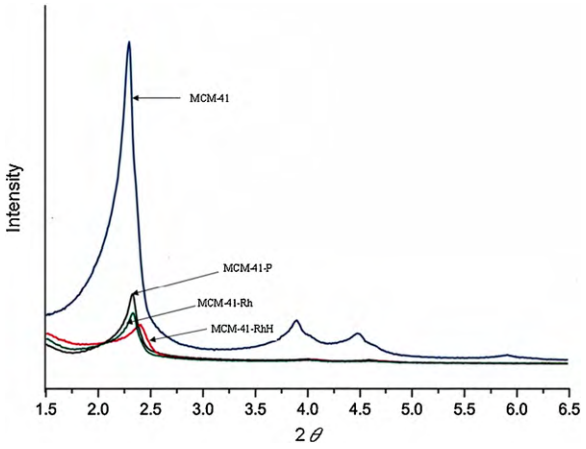

Fig. 1. Powder X-ray spectra of MCM-41, MCM-41-P, MCM-41-Rh and MCM-41-RhH.

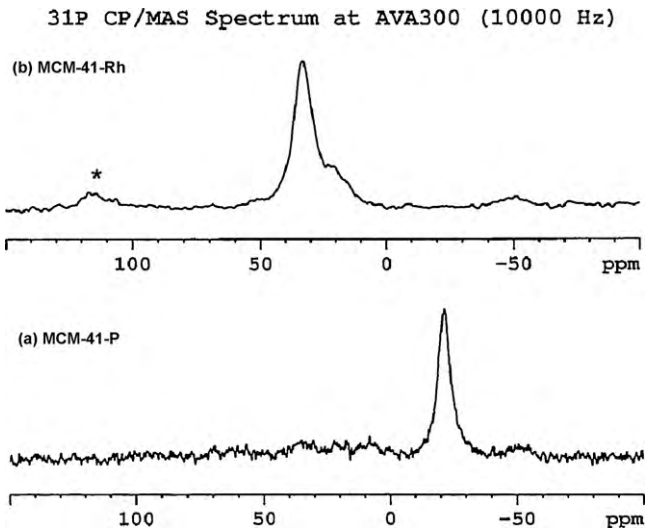

Fig. 2. Solid State ^{31}P NMR spectra of (a) MCM-41-P and (b) MCM-41-Rh. ^{31}P one-pulse experiments were performed on a Bruker Avance 300 spectrometer at a ^{31}P frequency of 121.49 MHz at ambient temperature. Chemical shifts were referenced to the isotropic chemical shift of H_3PO_4 at 0 ppm. Signals due to side spin bands are marked with asterisks.

spectroscopy (EDS) spectrum of the MCM-41-P suggests that it contains phosphorus, and a signal at −23.2 ppm in its solid state ^{31}P NMR further indicates that the ligand has been successfully anchored to the material. Oxidation of the phosphine is limited as indicated by the absence of the oxidized signal at 38 ppm [33]. The 18.0 Å pore size is still big enough for the passage of Rh catalyst through the pores in the latter anchoring process.

3.2. Preparation and characterization of the hybrid catalyst

Larger amount of hybrid catalyst MCM-41-Rh was prepared such that characterization and reactivity measurement could be obtained from the same batch of catalyst. The triphenyl phosphine ligands in $Rh(PPh_3)_3Cl$ are labile and can be substituted by other phosphine ligands. Immobilization of $Rh(PPh_3)_3Cl$ on MCM-41-P can therefore be achieved by the substitution of the triphenylphosphine with the tethered phosphine ligand $\equiv Si(CH_2)_3PPh_2$ on MCM-41-P. MCM-41-P was stirred in the benzene solution of $Rh(PPh_3)_3Cl$ for 48 hrs. After separation and washing, a yellowish powder of the hybrid catalyst (denoted as MCM-41-Rh) was obtained. EDS and WDS of MCM-41-Rh clearly indicate the presence of Rh and P. Powder X-ray diffraction of MCM-41-Rh shows a 38.0 Å $d(1\,0\,0)$ spacing diffraction signal (Fig. 1). The BET surface area is reduced to 304 m^2/g. Its uniform pore size of 17.5 Å is similar to that of MCM-41-P. All these show that the hybrid catalyst has a mesoporous structure (Table 1).

Solid state ^{31}P NMR spectra of the MCM-41-P and MCM-41-Rh were taken (Fig. 2). Before immobilization, the signal of the phosphorous of the tethered phosphine ligand is at −23.2 ppm. After immobilization, a broad resonance peak at 35 ppm is observed instead. In addition, the wavelength-dispersive spectrum (WDS) of MCM-41-Rh suggests that it contains rhodium. These observations indicate that $Rh(PPh_3)_3Cl$ has been successfully immobilized on MCM-41 [33]. The ^{31}P NMR of another sample showing both the signals of the tethered phosphine and the immobilized Rh complex further supports the above argument [13]. The Rh content (in weight %) of the hybrid catalyst is 2.1% by ICP-AES. The phosphorous contents (in weight %) are 1.3% for MCM-41-P and 2.8% for MCM-41-Rh.

3.3. Catalytic activity of the hybrid catalyst

The activity of this catalyst (20.1 mg) was evaluated by the hydrogenation of cyclohexene at 75 °C under 150 psi of hydrogen with toluene as the solvent (1.6 M). The TOF frequency of the catalyst is 2.0 s^{-1}. Under the same reaction conditions, the TOF of the $Rh(PPh_3)_3Cl$ (3.7 mg, 4.0×10^{-3} mmole) is 1.0 s^{-1}. These results are similar to the previous reported data [13].

The reasons for higher TOF for the hybrid catalyst than that of the homogeneous catalyst are still unclear. However, the present results may suggest that MCM-41-Rh is not always intact, and the raw species may be deformed. Hydrogenation reaction may induce significant migration and coalesce of the immobilized Rh complexes to more stable ones, thereby altering the catalytic properties. To confirm the suggestion, the structures of the fresh and used immobilized Rh catalysts were characterized by EXAFS spectroscopy.

As reported previously, it takes some time to pre-activate the catalyst during the initial period of the hydrogenation reaction [13]. In order to investigate the structure of the catalyst during the catalytic reaction, a larger amount of catalyst MCM-41-Rh was used in the hydrogenation reaction. The catalyst was recovered (denoted as MCM-41-RhH) after the hydrogenation reaction. The powder X-ray diffraction of MCM-41-RhH shows a 37.0 Å $d(1\,0\,0)$ spacing diffraction signal. Both the pore size distribution (18.0 Å) and surface area (308 m^2/g) of MCM-41-RhH by BET surface measurement are similar to the corresponding values of MCM-41-Rh before hydrogenation indicating the conservation of the mesoporous structure of the catalyst during the catalytic reaction (Table 1). The 18.0 Å pore size is still big enough for the passage of reactant, product, and even the Rh catalyst through the pores during the reaction.

3.4. EXAFS analysis of the hybrid catalyst before and after the hydrogenation reaction

Change of the ^{31}P NMR resonance position of the tethered phosphine ligand and the presence of signals of Rh in WDS after the reaction between MCM-41-P and $Rh(PPh_3)_3Cl$ only indicate the success of immobilization. One cannot conclude that the immobilized Rh complex has the structure $Rh(PPh_3)_2LCl$ or $Rh(PPh_3)L_2Cl$, with one or two of the triphenylphosphine ligand in $Rh(PPh_3)_3Cl$ being replaced by the tethered phosphine L. Because EXAFS analysis can provide information of the Rh local environment, EXAFS measurements of $Rh(PPh_3)_3Cl$, MCM-41-Rh, and MCM-41-RhH (the hybrid catalyst after hydrogenation) at Rh edge were carried out. The raw EXAFS data are shown in Fig. 3.

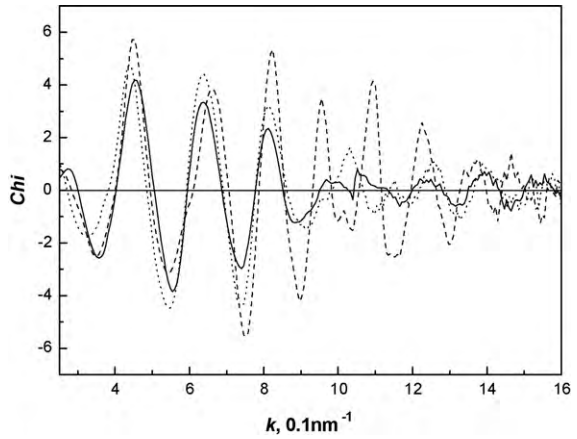

Fig. 3. Raw EXAFS data for $Rh(PPh_3)_3Cl$ (solid line), MCM-41-Rh (dotted line), and MCM-41-RhH (dashed line).

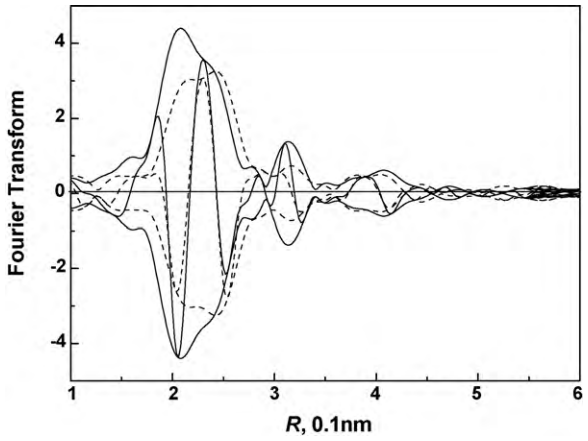

Fig. 4. Imaginary part and magnitude of Fourier transform (k^3-weighted, $3.5\,Å^{-1} < k < 14.0\,Å^{-1}$, Rh–P phase corrected) for MCM-41-Rh (solid line) and $Rh(PPh_3)_3Cl$ (dashed line).

Prior to the detailed EXAFS analysis of data characterizing samples of MCM-41-Rh and MCM-41-RhH, k^3-weighted Rh–P phase-corrected Fourier transform was determined for the EXAFS function. The Fourier transform provides qualitative information about the structure of the immobilized $Rh(PPh_3)_3Cl$ on MCM-41 (Fig. 4) [23,24]. The comparison of the Rh–P phase-corrected Fourier transform of $Rh(PPh_3)_3Cl$ with that of MCM-41-Rh shows that the contributions of the Rh–P and Rh–Cl for these two samples are hard to be differentiated in the imaginary part. However,

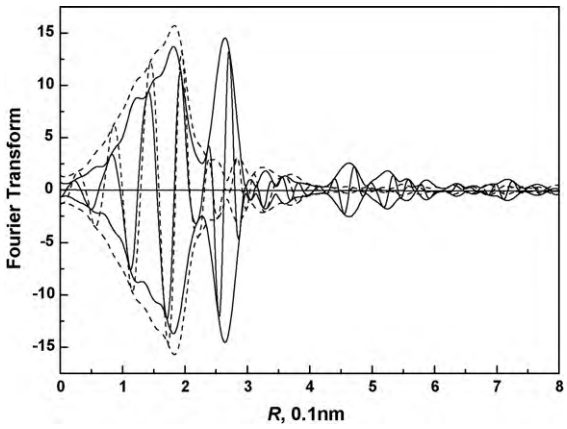

Fig. 5. Imaginary part and magnitude of Fourier transform (k^3-weighted, $3.5\,Å^{-1} < k < 14.0\,Å^{-1}$, Rh–Rh phase and amplitude corrected) for MCM-41-Rh (dashed line) and MCM-41-RhH (solid line).

the magnitude of the peak at about 2.5 Å in the Fourier transform of $Rh(PPh_3)_3Cl$ diminishes concomitantly with two new peaks appearing at about 2.0 Å and 3.1 Å in that of MCM-41-Rh. The peaks at 2.0 Å and 3.1 Å may contribute to the interactions of Rh complexes with MCM-41, and are temporarily assigned as Rh–O and Rh–Si interactions, respectively.

Some important surface chemistry involved in the hydrogenation reaction can be obtained from the Fourier transform of the EXAFS functions characterizing the structure of MCM-41-Rh and MCM-41-RhH. Fig. 5 shows the Rh–Rh phase and amplitude-corrected Fourier transform of EXAFS functions for MCM-41-Rh, and MCM-41-RhH. These results indicate that peak intensity for EXAFS contributions with bond distance less than 2.4 Å in MCM-41-Rh decreases with a new peak appearing at about 2.7 Å in MCM-41-RhH which is consistent with the Rh–Rh bond distance [34–37]. The appearance of Rh–Rh contributions is accounted for the reductive-oligomerization of the Rh complexes while the decrease of the amplitude of the peak at about 2.0 Å indicates the cleavage of the bonding between Rh and triphenylphosphine ligands. Important points raised by the preliminary analysis will be addressed below in the detailed EXAFS analysis section.

3.5. Detailed EXAFS analysis for MCM-41-Rh

A k^3-weighted Fourier transform without correction was performed on the EXAFS function over the range $2.73\,Å^{-1} < k < 14.41\,Å^{-1}$. The major contributions were isolated by inverse Fourier transform of the data in the range $1.17\,Å < R < 3.26\,Å$. Since Rh–O and Rh–P contributions are strongly coupled, the coarse

Table 2
Summary of EXAFS analysis results for MCM-41-Rh and MCM-41-RhH.

Shell	N[a]	R[b] (Å)	$1000 \times \Delta\sigma^2$[c] (Å^2)	ΔE_o[d] (eV)	EXAFS reference
MCM-41-Rh					
Rh–O	1.0 ± 0.3	2.01 ± 0.01	4 ± 2	10 ± 1	$Rh–O_{exp}$
Rh–P	2.1 ± 03	2.27 ± 0.02	1 ± 1	4 ± 2	$Rh–P_{exp}$
Rh–Si	0.8 ± 0.2	3.15 ± 0.02	2 ± 2	4 ± 2	$Rh–Si_{feff}$
MCM-41-RhH					
Rh–O	0.8 ± 0.3	1.99 ± 0.01	3 ± 2	3 ± 2	$Rh–O_{exp}$
Rh–P	2.4 ± 0.3	2.27 ± 0.02	1 ± 1	4 ± 1	$Rh–P_{exp}$
Rh–Si	0.6 ± 0.2	3.11 ± 0.02	1 ± 2	6 ± 2	$Rh–Si_{feff}$
$Rh–Rh_{1st}$	1.3 ± 0.2	2.68 ± 0.01	4 ± 1	5 ± 1	$Rh–Rh_{feff}$
$Rh–Rh_{2nd}$	0.7	4.65 ± 0.03	4 ± 2	9 ± 3	$Rh–Rh_{feff}$

[a] N, the coordination number for the absorber–backscattering pair.
[b] R, the average absorber–backscattering distance.
[c] $\Delta\sigma^2$, the difference in Debye–Waller factors between sample and standard.
[d] ΔE_0, the inner potential correction.

structural parameters characteristic of these two contributions were estimated by fitting the isolated EXAFS function in the range 3.5 Å^{-1} < k < 14.0 Å^{-1}. The EXAFS function for the Rh–O contribution was calculated from the coarsely estimated structural parameters and was subtracted from the Fourier isolated major contributions. The residual spectrum was expected to represent Rh–P, Rh–Cl, and Rh–Si contributions. However, after a k^3-weighted Rh–P phase-corrected Fourier transformation was performed on the residual spectrum, only two major peaks appeared at 2.2 Å and 3.1 Å in R space. The structural parameters characteristic of these two contributions (Rh–P and Rh–Si) were then fitted the residual data. The calculated Rh–P and Rh–Si EXAFS functions were then subtracted from the isolated data and better parameters for Rh–O were estimated. The refinement through this iteration was continued until good overall agreement was obtained. The criterion of a satisfactory fit is based on the comparison between experimental and calculated results with k^1 and k^3 weighting in R space.

The final results are summarized in Table 2, and the comparisons of the data with the fit are shown in Fig. 6a and b. In addition, as shown in Fig. 6c–e, the imaginary part of the Fourier transform of each contribution is rather positive and symmetrical (Fig. 6c–e), confirming the identification of backscattering atoms proposed by preliminary analysis [24]. The small peak at about 2.45 Å shown in Fig. 6e is Rh–Cl contribution. This contribution is too small to esti-

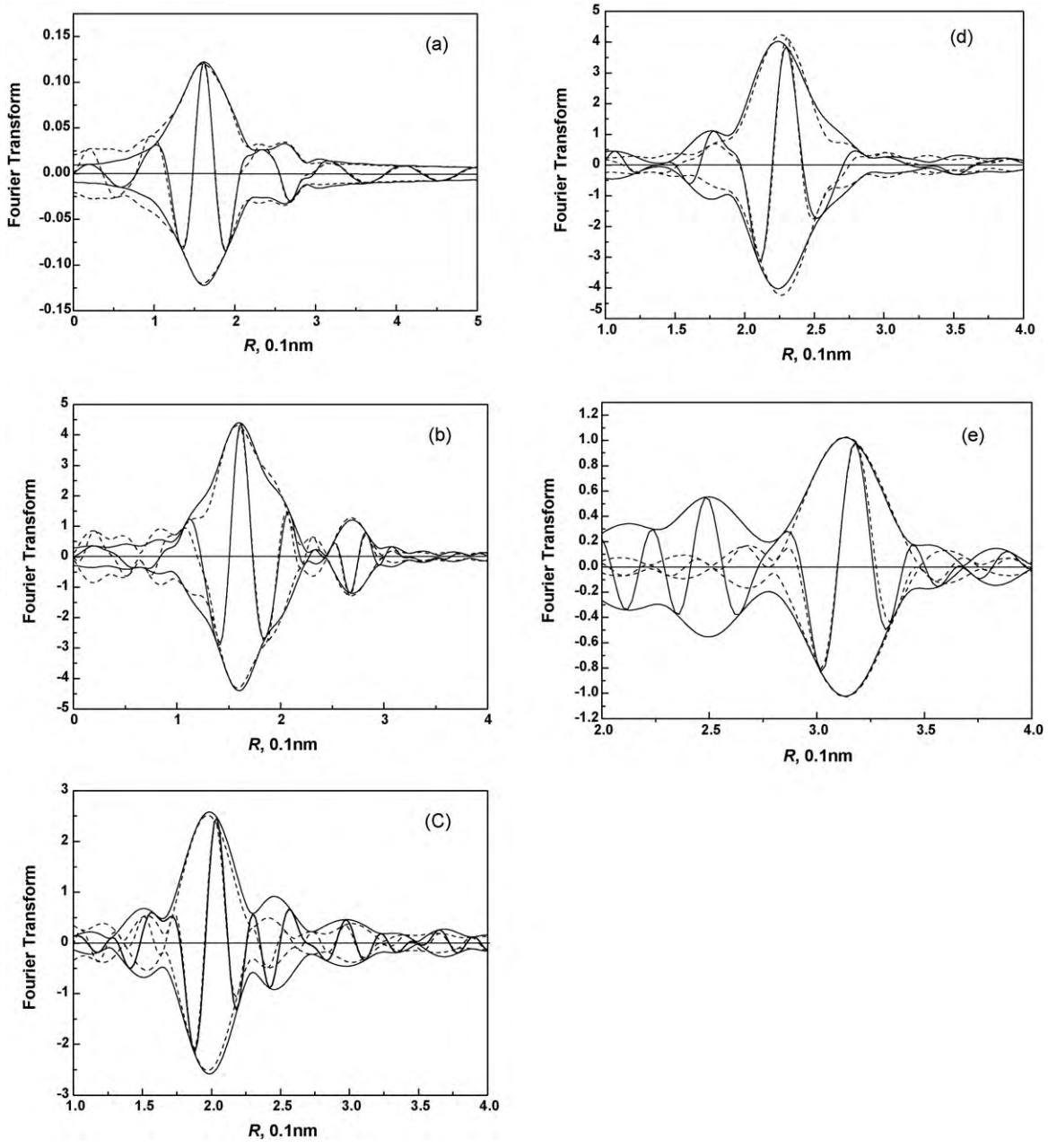

Fig. 6. Results of EXAFS analysis obtained with the best calculated structural parameters for MCM-41-Rh. (a) Fourier transform (k^1-weighted, 3.5 Å^{-1} < k < 14.0 Å^{-1}) of experimental EXAFS (solid line) and sum of the calculated Rh–O, Rh–P, and Rh–Si contributions (dashed line), (b) Fourier transform (k^3-weighted, 3.5 Å^{-1} < k < 14.0 Å^{-1}) of experimental EXAFS (solid line) and sum of the calculated Rh–O, Rh–P, and Rh–Si contributions (dashed line), (c) Fourier transform (k^3-weighted, 3.5 Å^{-1} < k < 14.0 Å^{-1}, Rh–O phase corrected) of experimental EXAFS minus calculated Rh–P and Rh–Si EXAFS (solid line) and the calculated Rh–O EXAFS (dashed line), (d) Fourier transform (k^3-weighted, 3.5 Å^{-1} < k < 14.0 Å^{-1}, Rh–P phase corrected) of experimental EXAFS minus calculated Rh–O and Rh–Si EXAFS (solid line) and the calculated Rh–P EXAFS (dashed line) and (e) Fourier transform (k^3-weighted, 3.5 Å^{-1} < k < 14.0 Å^{-1}, Ph–Si phase corrected) of experimental EXAFS minus calculated Rh–O and Rh–P EXAFS (solid line) and the calculated Rh–Si EXAFS (dashed line).

mate the structural parameters, whereas it indicates the existence of trace chloride ligand bonded to Rh.

3.6. Detailed EXAFS analysis for MCM-41-RhH

A preliminary EXAFS analysis shows the formation of Rh oligomers after the hydrogen reaction. In order to examine the existence of high Rh–Rh shell, instead of isolating major contributions by Fourier filter technique, raw EXAFS data were used for the fit. At the beginning, the contributions of Rh–O and Rh–P were extracted by Fourier filter in the range 0.5 Å < R < 2.2 Å of the Rh–Rh phase and amplitude-corrected EXAFS function (Fig. 7). The coarse structural parameters characterizing these two contributions were estimated by XDAP fitting routine with the structural parameters of MCM-41-Rh as initial guess. Rh–O and Rh–P contributions calculated from these coarse parameters were subtracted from raw EXAFS data. The residual spectrum is mainly Rh–Rh and Rh–Si contributions. The structural parameters characteristic of these contributions were then estimated by fitting the k^2-weighted data in 2.0 Å < R < 5.0 Å. The Rh–Rh and Rh–Si contributions were subtracted from the raw data, and better parameters for Rh–P and Rh–O were estimated. The recursive iterations were carried out until a satisfactory overall fit was reached.

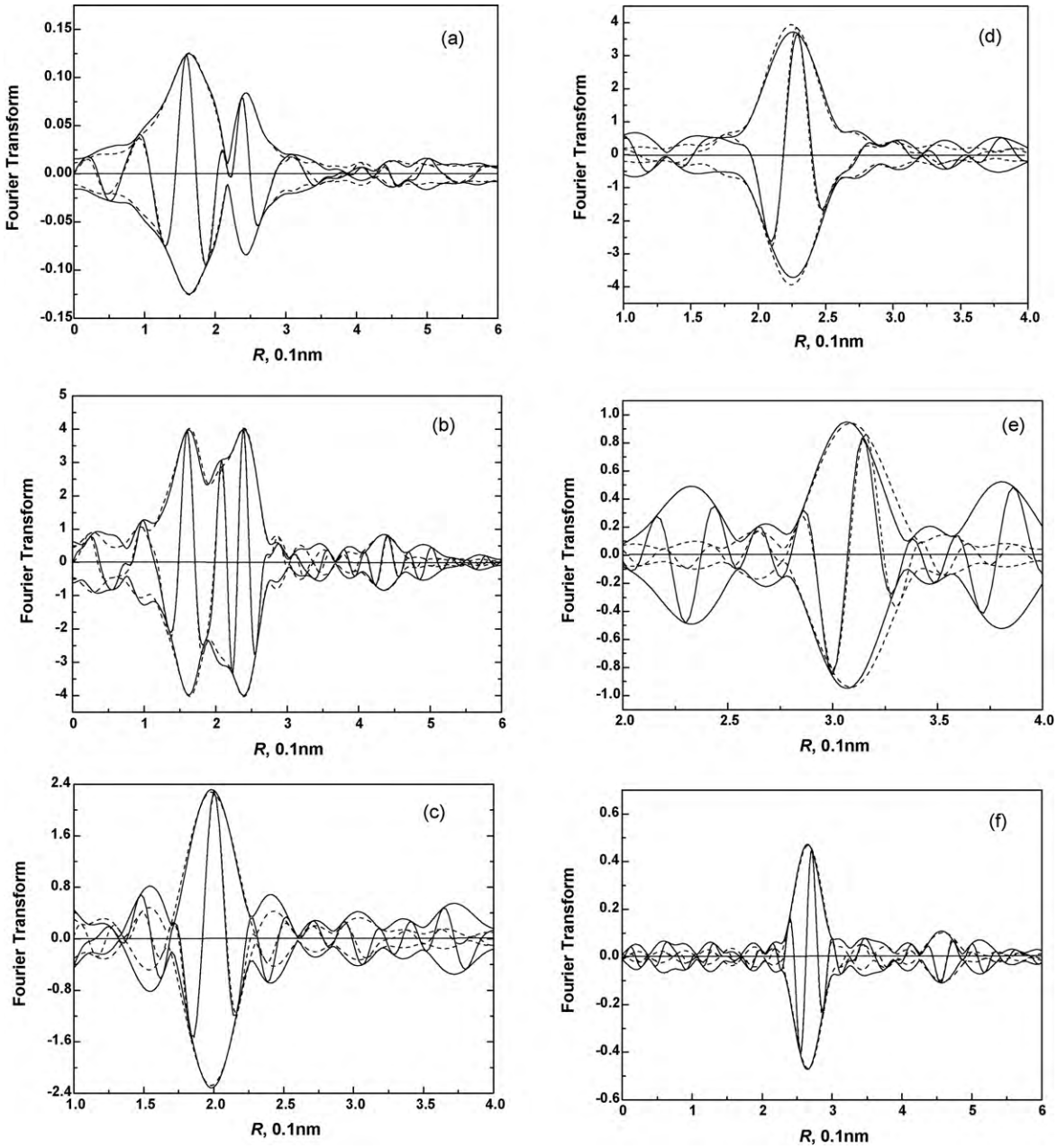

Fig. 7. Results of EXAFS analysis obtained with the best calculated structural parameters for MCM-41-RhH. (a) Fourier transform (k^1-weighted, 3.5 Å^{-1} < k < 14.0 Å^{-1}) of experimental EXAFS (solid line) and sum of the calculated Rh–O, Rh–P, Rh–Si, and Rh–Rh contributions (dashed line), (b) Fourier transform (k^3-weighted, 3.5 Å^{-1} < k < 14.0 Å^{-1}) of experimental EXAFS (solid line) and sum of the calculated Rh–O, Rh–P, Rh–Si and Rh–Rh contributions (dashed line), (c) Fourier transform (k^3-weighted, 3.5 Å^{-1} < k < 14.0 Å^{-1}, Ph–O phase corrected) of experimental EXAFS minus calculated Rh–P, Rh–Rh and Rh–Si EXAFS (solid line) and the calculated Rh–O EXAFS (dashed line), (d) Fourier transform (k^3-weighted, 3.5 Å^{-1} < k < 14.0 Å^{-1}, Rh–P phase corrected) of experimental EXAFS minus calculated Rh–O, Rh–Rh and Rh–Si EXAFS (solid line) and the calculated Rh–P EXAFS (dashed line), (e) Fourier transform (k^3-weighted, 3.5 Å^{-1} < k < 14.0 Å^{-1}, Rh–Si phase corrected) of experimental EXAFS minus calculated Rh–O, Rh–Rh and Rh–P EXAFS (solid line) and the calculated Rh–Si EXAFS (dashed line) and (f) Fourier transform (k^2-weighted, 3.5 Å^{-1} < k < 14.0 Å^{-1}, Rh–Rh phase and amplitude corrected) of experimental EXAFS minus calculated Rh–O, Rh–Si and Rh–P EXAFS (solid line) and the calculated Rh–Rh EXAFS (dashed line).

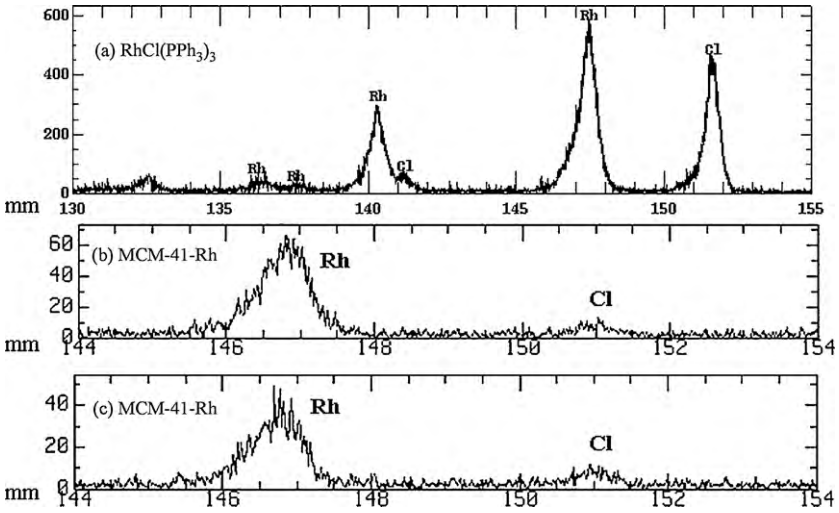

Fig. 8. WDS analysis of (a) $RhCl(PPh_3)_3$, (b) MCM-41-Rh and (c) MCM-41-RhH.

The final results are summarized in Table 2 and the comparisons of the data with the fit are shown in Fig. 7a and b. The calculated and experimental contribution for Rh–O, Rh–P, and Rh–Si are shown in Fig. 7c–e, respectively. Except second Rh–Rh contribution, the characteristic peaks for each shell are positive and symmetrical (Fig. 7c and d), confirming the identification of backscattering atom [24]. The asymmetrical peak for the second Rh–Rh contribution suggests that this peak may be from other contributions such as Rh–C and interactions between Rh and MCM-41. However, the characteristic peaks for these contributions are strongly coupled with each other and are too small to be analyzed.

3.7. Structures of MCM-41-Rh and MCM-41-RhH and reasons for low leaching rate

Combining with NMR results, we suggest that the substitution of triphenylphosphine ligand with the tethered phosphine ligand and a Rh–O–Si linkage [35] immobilize the Rh complexes on MCM-41 surface. However, the immobilized Rh complexes is not very stable, olefin hydrogenation reaction induces oligomerization of the Rh complexes with the elimination of PPh_3 ligand. WDS analysis of both MCM-41-Rh and MCM-41-RhH indicating the Cl contains of both samples are substantially reduced as compared to the WDS of $Rh(PPh_3)_2Cl$ (Fig. 8). These observations further confirm the formation of Rh–O–Si bonding with the elimination of the Cl ligand on $Rh(PPh_3)_2Cl$. In addition, formation of Rh–O–Si bonding has been observed in the reaction between Rh complex and surface Si–OH [35].

Based on the results of EXAFS analysis, we conclude that a monomeric Rh species anchored to the support through the Rh–O–Si and Rh–L (L = tethered phosphine ligand) linkages before hydrogenation. The other ligands are phosphine ligands as indicated by the EXAFS analysis. Possible structure of MCM-41-Rh is shown in Scheme 1. After hydrogenation, Fourier transform of EXAFS functions for MCM-41-RhH shows peaks at about 2.7 Å and is consistent with Rh–Rh bond distance implying the formation of Rh–Rh bonding (Fig. 5). The $Rh–Rh_{1st}$ shell coordination number of 1.3 (Table 2) suggests dimeric Rh species are formed on MCM-41 surface. In addition, Rh–O coordination number of 0.8 ± 0.3 indicates that Rh species is anchored to the support oxide surface with only one $Rh–O_{support}$ bond.

The second Rh–Rh shell with bond distance of 3.83 Å is an indication of a 3-dimensional character of Rh clusters. Since no significant peaks are observed in the range of 3.5 Å < R < 4.0 Å for Rh–Rh phase and amplitude-corrected Fourier transform of the experimental EXAFS minus the contribution of Rh–O, Rh–Si and Rh–P (Fig. 7f), metal cluster is unlikely formed. Combined the structure model with activity test results, the activity enhancement after first reaction cycle is regarded to be caused by the formation of dimeric species. However, the effects of trace metal clusters formed on MCM-41 surface cannot be ruled out completely because rather small characteristic peak for the second Rh–Rh shell may be covered by noise.

According to WDS analysis, small amount of Cl still exists in both MCM-41-Rh and MCM-41-RhH. EXAFS analysis indicates that small among of Cl is coordinated to the Rh in both samples. All these show the presence of small amount of species with chloride ligand on the support before and after hydrogenation reaction. This may be $Rh(PPh_3)LCl$ (L = tethered phosphine ligand) or other unknown species. However, the active Rh catalyst in the hybrid catalyst is no longer preserving the monomeric structure similar to $Rh(PPh_3)_3Cl$. This may imply that MCM-41-RhH, which is produced after the first catalytic cycle, is the actual catalyst.

The low leaching rate in the hydrogenation reaction is understandable. The Rh–O–Si bonding is unlikely to break during the hydrogenation reaction. The coordination of the tethered phosphine to the Rh is reversible, and the tethered phosphine may be detached from the metal, and the empty coordination site could be occupied by any coordination molecules such as olefin. However, the coordination ability of olefin is weaker than that of phosphine, and the reattachment process through the substitution of the coordinated olefin with the tethered phosphine can resume the immobilization status. In addition, the channel of the mesoporous support is around 20 Å i.d. and a few microns in length, and the concentration of the tethered phosphine is very high in the channel. If there is any leaching, the free Rh complex can be readily immobilized by substitution of the olefin ligand with the other tethered phosphine ligand in the same channel. Leaching of this free Rh complex is thus suppressed.

4. Conclusions

Immobilization of $Rh(PPh_3)_3Cl$ on a phosphinated mesoporous MCM-41 produces a hybrid catalyst MCM-41-Rh for hydrogenation of cyclohexene. Solid state ^{31}P NMR and WDS of MCM-41-Rh indicate the success of immobilization. Monomeric structure with an Rh–O–Si linkage to the support is proposed for the immobilized Rh species based on the EXAFS analysis results which shows Rh–O

and Rh–Si interactions of 2.01 Å and 3.15 Å, respectively. Because of these Rh-support interactions, leaching of Rh is limited during the catalytic hydrogenation reaction cycles. As opposed to $Rh(PPh_3)_3Cl$, the much higher catalyst activity is mostly caused by the formation of dimeric Rh species during hydrogenation. However, enhancement contributed from trace of Rh metal clusters may not be ruled out.

Acknowledgements

We acknowledge supports from Academia Sinica program project on "Novel catalysts for the activation of small important molecules", Academia Sinica nanoprogram and National Science Council. We also thank Dr. Yoshiyuki Iizuka in the Laboratory of Electron Probe Micro-Analyses of the Institute of Earth Sciences, Academia Sinica for obtaining the WDS spectra and Dr. Jyh-Fu Lee for the help in performing EXAFS experiments. The EXAFS data were analyzed using the FEFF and XDAP Data Analysis Program. XDAP Program was developed by M. Vaarkam, J.C. Linders, and D.C. Koningsberger.

References

[1] J.A. Gladysz, Chem. Rev. 102 (2002) 3215–3216.
[2] Y. Iwasawa, Tailored Metal Catalysts, D. Reidel Publishing Company, Dordrecht, Holland, 1986, p. 1.
[3] K.G. Allum, R.D. Hancock, I.V. Howell, R.C. Pitkethly, P.J. Robinson, J. Organomet. Chem. 87 (1975) 189–201.
[4] K.G. Allum, R.D. Hancock, I.V. Howell, S. McKenzie, R.C. Pitkethly, P.J. Robinson, J. Organomet. Chem. 87 (1975) 203–216.
[5] C.T. Kresge, M.E. Leonowicz, W.J. Roth, J.C. Vartuli, J.S. Beck, Nature 359 (1992) 710–712.
[6] D.E. De Vos, M. Dams, B.F. Sels, P.A. Jacobs, Chem. Rev. 102 (2002) 3615–3640.
[7] J.S. Beck, J.C. Vartuli, W.J. Roth, M.E. Leonowicz, C.T. Kresge, K.D. Schmitt, C.T.-W. Chu, D.H. Olson, E.W. Sheppard, S.B. McCullen, J.B. Higgins, J.L. Schlenker, J. Am. Chem. Soc. 114 (1992) 10834–10843.
[8] W. Zhou, J.M. Thomas, D.S. Shephard, B.F.G. Johnson, D. Ozkaya, T. Maschmeyer, R.G. Bell, Q. Ge, Science 280 (1998) 705–708.
[9] T. Maschmeyer, F. Rey, G. Sankar, J.M. Thomas, Nature 378 (1995) 159–162.
[10] C.-J. Liu, S.-G. Li, W.-Q. Pang, C.-M. Che, Chem. Commun. (1997) 65–66.
[11] R. Anwander, Chem. Mater. 13 (2001) 4419–4438.
[12] A. Taguchi, F. Schüth, Micropor. Mesopor. Mater. 77 (2005) 1–45.
[13] S.-G. Shyu, S.-W. Cheng, D.-L. Tzou, Chem. Commun. (1999) 2337–2338.
[14] C.M. Crudden, D. Allen, M.D. Mikoluk, J. Sun, Chem. Commun. (2001) 1154–1155.
[15] F.M. De Rege, D.K. Morita, K.C. Ott, W. Tumas, R.D. Broene, Chem. Commun. (2000) 1797–1798.
[16] L. Huang, S. Kawi, J. Mol. Catal. A 211 (2004) 23–33.
[17] L. Huang, S. Kawi, Catal. Lett. 90 (2003) 165–169.
[18] C. Merckle, S. Haubrich, J. Blumel, J. Organomet. Chem. 627 (2001) 44–54.
[19] B.C. Gates, Catalytic Chemistry, John Wiley & Sons, Inc., 1992, p. 343.
[20] C.-F. Cheng, D.H. Park, J. Klinowski, J. Chem. Soc., Faraday Trans. 93 (1997) 193–197.
[21] H.-M. Lin, S.-T. Kao, K.-M. Lin, J.-R. Chang, S.-G. Shyu, J. Catal. 224 (2004) 156–163.
[22] M.-T. Tang, T.-E. Dann, C.-C. Chen, K.-L. Tsang, C.T. Chen, K.S. Liang, Nucl. Instrum. Methods Phys. Res. Sect. A 467/468 (2001) 719–722.
[23] M. Vaarkamp, J.C. Linders, D.C. Koningsberger, Physica B 208–209 (1995) 159–160.
[24] D.C. Koningsberger, R. Prins, X-ray Absorption: Principles, Applications, Techniques of EXAFS, SEXAFS, and XANES, Wiley, New York, 1988, pp. 211–253.
[25] M. Vaarkamp, I. Dring, R.J. Oldman, E.A. Stern, D.C. Koningsberger, Phys. Rev. B 50 (1994) 7872–7883.
[26] J.W. Cook, D.E. Sayers, J. Appl. Phys. 52 (1981) 5024–5031.
[27] J.B.A.D. Van Zon, D.C. Koningsberger, H.F.J. Van't Blik, D.E. Sayers, J. Chem. Phys. 82 (1985) 5742–5754.
[28] S.I. Zabinsky, J.J. Rehr, A. Ankudinov, R.C. Albers, M.J. Eller, Phys. Rev. B 52 (1995) 2995–3009.
[29] A.L. Ankudinov, B.J. Ravel, J. Rehr, S.D. Conradson, Phys. Rev. B 58 (1998) 7565–7576.
[30] X. Feng, G.E. Fryxell, L.–Q. Wang, A.Y. Kim, J. Liu, K.M. Kemner, Science 276 (1997) 923–926.
[31] R.H. Grubbs, L.C. Kroll, J. Am. Chem. Soc. 93 (1971) 3062–3063.
[32] K.G. Allum, R.D. Hancock, I.V. Howell, T.E. Lester, S. McKenzie, R.C. Pitkethly, P.J. Robinson, J. Catal. 43 (1976) 331–338.
[33] J. Kramer, E. Nollen, W. Buijs, W.L. Driessen, J. Reedijk, React. Funct. Polym. 57 (2003) 1–11.
[34] M. Pillinger, C.D. Nunes, P.D. Vaz, A.A. Valents, I.S. Goncalves, P.J.A. Ribeiro-Claro, J. Rocha, L.D. Carlos, F.E. Kühn, Phys. Chem. Chem. Phys. 4 (2002) 3098–3105.
[35] K. Asakura, K. Kitamura-Bando, K. Isobe, H. Arakawa, Y. Iwasawa, J. Am. Chem. Soc. 112 (1990) 3242–3244.
[36] K.R. Dunbar, J. Am. Chem. Soc. 110 (1988) 8247–8249.
[37] S.G. Fiddy, J. Evans, T. Neisius, X.-Z. Sun, Z. Jie, M.W. George, Chem. Commun. (2004) 676–677.